Title

Optimized culture system to induce neurite outgrowth from retinal ganglion cells in three-dimensional retinal aggregates differentiated from mouse and human embryonic stem cells

Authors

Yuki Maekawa[1,2], Akishi Onishi[1], Keizo Matsushita[1,3], Naoshi Koide[1], Michiko Mandai[1], Kiyoshi Suzuma[2], Takashi Kitaoka[2], Atsushi Kuwahara[4], Chikafumi Ozone[4], Tokushige Nakano[4], Mototsugu Eiraku[5], Masayo Takahashi[1]

[1]Laboratory for Retinal Regeneration, RIKEN Center for Developmental Biology

[2]Department of Ophthalmology and Visual Science, Graduate School of Biomedical Science, Nagasaki University

[3]Regenerative and Cellular Medicine Office, Sumitomo Dainippon Pharma Co., Ltd

[4]Neurogenesis and Organogenesis Group, RIKEN Center for Developmental Biology

[5]Four-Dimensional Tissue Analysis Unit, RIKEN Center for Developmental Biology

Corresponding author:

Akishi Onishi, PhD

Laboratory for Retinal Regeneration, RIKEN Center for Developmental Biology

2-2-3 Minatojima-minamimachi, Chuo, Kobe 650-0047, Japan

Tel: +81-78-306-3305, Fax: +81-78-306-3303

Email: aonishi@cdb.riken.jp

ABSTRACT

Purpose

To establish a practical research tool for studying the pathogenesis of retinal ganglion cell (RGC) diseases, we optimized culture procedures to induce neurite outgrowth from three-dimensional self-organizing optic vesicles (3D-retinas) differentiated *in vitro* from mouse and human embryonic stem cells (ESCs).

Materials and methods

The developing 3D-retinas isolated at various time points were placed on Matrigel-coated plates and cultured in media on the basis of the 3D-retinal culture or the retinal organotypic culture protocol. The number, length, and morphology of the neurites in each culture condition were compared.

Results

First, we confirmed that Venus-positive cells were double-labeled with a RGC marker, Brn3a, in the 3D-retina differentiated from Fstl4::Venus mouse ESCs, indicating specific RGC-subtype differentiation. Second, Venus-positive neurites grown from these RGC subsets were positive for beta-III tubulin and SMI312 by immunohistochemistry. Enhanced neurite outgrowth was observed in the B27-supplemented Neurobasal-A medium on Matrigel-coated plates from the optic vesicles isolated after 14 days of differentiation from mouse ESCs. For the differentiated RGCs from human ESCs, we obtained neurite extension of >4 mm by modifying Matrigel coating and the culture medium from the mouse RGC culture.

Conclusion

We successfully optimized the culture conditions to enhance lengthy and high-frequency neurite outgrowth in mouse and human models. The procedure would be useful for not only developmental studies of RGCs, including maintenance and

projection, but also clinical, pathological, and pharmacological studies of human RGC diseases.

INTRODUCTION

Mammalian retinas are composed of five types of neurons with three neuronal layers. Retinal ganglion cells (RGCs) are localized to the layer of the vitreous side (ganglion cell layer), and long axons from RCGs extend to various brain areas[1]. As RGCs are the only pathways by which external signals are transmitted from the retina to the brain, RGC injury and/or diseases directly lead to visual disturbances. The mechanism underlying RGC impairment has been investigated using organotypic or dissociated culture systems[2]. The neurites from RGCs have been examined to assess their outgrowth, projections, and maintenance as well as molecular responses; this is because these experiments provided essential information for developmental, pathological, and physiological studies[3,4]. However, researchers have to consider the species differences underlying morphological and developmental characteristics such as RGC subtypes[5]. In addition, although there have been various human RGC disorders[6], the *ex vivo* approaches, particularly those with human models, include ethical issues. A few groups have examined retinal explant cultures isolated from postmortem adults and reported low viability and undetectable neurite outgrowth[7-9].

Recently, to overcome such limitations, several *in vitro* methods to differentiate RGCs from embryoid bodies of mouse or human pluripotent stem cells have been proposed[10-13]. Eiraku et al. reported the development of a retinal serum-free floating culture of embryoid body-like aggregates with quick reaggregation (SFEBq) culture; this provided three-dimensional self-organizing optic vesicle-like

structures (3D-retina) with layered retinal neurons[14]. Each procedure had previously confirmed pandifferentiation RGC markers, including Brn3a and/or Brn3b, which are responsible for dendritic stratification, maintenance, and projections of RGCs[15-17]. However, because differentiated RGCs are classified into a number of subtypes depending on their physiological properties, morphology, central projections, and molecular markers[5,18-22], these *in vitro* differentiated RGCs should be characterized at the subtype level.

In this study, we validated the subtype specification of RGCs in the retinal SFEBq culture and optimized culture procedures so that neurites of RGCs in the optic vesicles would be enhanced and preserved. In the mouse model, we generated embryonic stem cells (ESCs) from Follistatin-like 4 (Fstl4)::Venus mice to visualize specific subtypes of RGCs and confirm neurite outgrowth. Using optic vesicles containing RGCs differentiated from mouse and human ESCs, we optimized each culture condition to induce the neurite outgrowth and successfully generated numerous and lengthy neurites from RGCs.

The neurite outgrowth obtained in our optimized culture procedure enables quantitative and qualitative analyses of RGCs, making it possible for us to assess the pathophysiological and pharmacological studies of mouse and human RGCs by minimizing animal sacrifice or purification procedures.

MATERIALS AND METHODS

Differentiation of 3D-retinas from mouse ESCs

Fstl4::Venus knock-in mice were obtained from RIKEN BioResource center (Tsukuba, Japan)[23] and treated in compliance with the Guidelines for Use of Laboratory Animals of RIKEN. Fstl4::Venus mouse ESCs were generated as

described previously[24,25]. Mouse ESCs of Fstl4::Venus and Rx::GFP[26,27] were maintained as reported previously[28], and 3D-optic vesicles were differentiated by the retinal SFEBq culture protocol[14] with minor modifications[29]. In brief, the embryoid bodies forming optic vesicle-like structures around differentiation days (DDs) 7 to 9 were transferred to floating cultures and maintained. Media were supplemented with 0.5 μM retinoic acid (RA, Sigma-Aldrich Corp., St. Louis, MO, USA) and 1 mM L-taurine (Wako Pure Chemical Industries, Osaka, Japan) from DD14[30] or after the placement of optic vesicles. Undifferentiation (Nanog and Oct4) and differentiation (Rx) marker expressions were confirmed by RT-PCR as described previously[29] (primers are listed in Supplemental Table 1).

Differentiation of 3D-retinas from human ESCs

Rx::Venus and *Crx*::Venus human ESCs distributed by Dr. Y. Sasai[31] were used in accordance with human ES cell research guidelines of Japanese government. Human ESCs were maintained and differentiated into the 3D-retinas as described previously[32]. In brief, ESCs dissociated by TrypLE Select (Life Technologies, Carlsbad, CA, USA) with 0.05 mg/mL DNaseI (Roche Diagnostics, Tokyo, Japan) and 20 μM Y-27632 (Wako) were resuspended in the growth factor-free chemically defined medium (gfCDM), containing IMDM:F12 (1:1, Life Technologies), 1× Chemically Defined Lipid Concentrate (Life Technologies), and 450 μM monothioglycerol (Sigma), supplemented with 10% knockout serum replacement (KSR) and 20 μM Y-27632. Twelve thousand cells per well were placed into low-cell adhesion V-bottomed 96-well plates (Sumitomo Bakelite, Tokyo, Japan). On DD6, the culture medium was changed to gfCDM containing 10% KSR and 1.5 nM bone morphogenetic protein 4 (BMP4). Half of the medium was

changed every 3 days to gfCDM containing 10% KSR. At DD18, the spheres forming optic vesicles were transferred to low-cell adhesion dishes (Sumitomo Bakelite) in DMEM/F12 (Life Technologies) containing 1% N2 supplement (Life Technologies) and 3 μM CHIR99021(Stemgent, Cambridge, MA, USA). The medium was changed at DD22–24 to DMEM/F12 containing 10% fetal bovine serum (FBS) (Biological Industries, Beit HaEmek, Israel), 1% N2, 0.5 μM RA, 0.1 mM L-taurine, and Antibiotic–Antimycotic (Life Technologies) until it was time to dissect the optic vesicles.

Neurite outgrowth on adhesion cultures

The Venus/GFP-positive optic vesicles (DD10–20 in mouse and DD46 in human models) excised under a fluorescent dissection microscope (Leica Microsystems, Wetzlar, Germany) were placed into 24-well plates or 0.4–1.0-μm microporous filter inserts (Corning, Corning, NY, USA) coated with growth factor reduced Matrigel (MG-GFR, Corning). For a thicker MG coating, culture vessels were covered with 1 μL/cm^2 of MG-GFR and solidified at 37°C for 1 h. For a thinner MG coating, containers were covered with 1.5–2 μL/cm^2 of 10% MG-GFR diluted in each substrate media and removed after 1 h of incubation at room temperature. The placed optic vesicles were cultured at 37°C in 40% O_2 and 5% CO_2 in N2-supplemented DMEM/F12 medium containing either 10% (D-F10), 1% (D-F1), and 0% (D-F0) of FBS or B27 supplement (D-B27, only for human samples, Life Technologies) or in Neurobasal-A medium (Life Technologies) containing B27 supplement and 1 mM L-glutamine (Sigma) (N-B27). All media were supplemented with 0.5 μM RA and 1 mM L-taurine as well as 100 U/mL penicillin and streptomycin (Life Technologies). To track neurite outgrowth, spheres were monitored by

IncuCyte™ (Essen BioScience, Ann arbor, MI, USA), a time-lapse live-cell imaging system built in the incubator that automatically took phase contrast and green fluorescent images every 6–8 h. Neurites were counted under an inverted microscope DM IL LED (Leica), and pictures were taken using an inverted fluorescence microscope IX71 (Olympus, Tokyo, Japan) as required. Culture media were changed every 2 days.

Measurement of neurites

The length of the neurites was measured from the pictures taken by IncuCyte™ at 5 days (mouse) or at 4 and 7 days (human) after placement and analyzed with ImageJ (1.48v, NIH, Bethesda, MD, USA). The five longest neurites from each optic vesicle were chosen and traced from the edge to the end on touchscreen displays. After the calculation, the lengths of the three longest neurites were statistically evaluated.

Immunohistochemistry and imaging

Three-dimensional retinal spheres fixed for 30 min in 3% paraformaldehyde/phosphate buffered saline (PBS) with 7.5% sucrose were cryoprotected in 30 % sucrose/PBS and embedded in O.C.T. compound (Sakura Finetek, Tokyo, Japan). Sections (10 μm) were immunostained with primary antibodies (Supplemental Table 2). For whole-mount immunostaining, the fixed 3D-retinas on filter inserts (Corning) were incubated for 2 h in 10% horse serum/PBS with 0.5% Triton X-100 (Wako) for blocking at room temperature and for 2 days in primary antibodies in 1% horse serum/PBS with 0.05% Triton X-100 at 4°C. Secondary antibodies conjugated with Alexa Fluor 488, 546, and 647 were incubated

for 1 day at 4°C. The samples were mounted in FluorSave™ Reagent (Merck Millipore, Darmstadt, Germany). All the images for both cryosections and whole-mount immunohistochemistry samples were obtained from Leica TCS SP8 (Leica).

Statistical analysis

All data were presented as mean ± standard deviation (S.D.). The numbers and length of neurites were analyzed by the Kruskal–Wallis one-way analysis of variance. A p value of <0.05 was considered to be statistically significant. If the result showed a significant difference, Dunn's post-hoc comparisons were made between all the pairs. Whole statistical analysis was performed using SPSS Statistics (version 22.0.0.0, IBM, Armonk, NY, USA).

RESULTS

Neurite outgrowth from Fstl4::Venus mouse ESCs

To follow neurite outgrowth specifically from RGCs, we generated ESCs from Fstl4::Venus-knock-in mice[23]. Fstl4 (also known as Spig1) has been reported to be expressed in two functionally distinct subtypes of RGCs: one was a direction-selective ON-type RGC, and the other was a lateral geniculate nucleus (LGN)-projecting RGC localized at the dorsal retina[33]. After confirming that the Fstl4::Venus ESCs exhibited the characteristic morphology and gene expression of pluripotency (Figure 1A and B), 3D-retinas were differentiated in our modified SFEBq culture that generated optic vesicle, preferentially contacting neural retinas[14,29,30]. Three-dimensional retinas examined 10 and 23 days after differentiation (DD10 and DD23) expressed Rx, a retinal progenitor marker, while pluripotency-related genes (Nanog and Oct4) were downregulated (Figure 1B). As reported previously[14,29,30], typical

optic vesicle structures with a clear neural epithelium were observed from around DD7–10 and gradually enlarged until DD20 (Figure 1D). Rhodopsin-positive cells were localized at the inner half of the neural epithelium of optic vesicles at DD20 (Figure 1C). Venus fluorescence was detectable around DD12 and enhanced by DD14 (Figure 1E).

Following this, we performed morphological and immunohistochemical analyses with Brn3a, an RGC marker. At DD10, Brn3a-positive cells were not observed but became detectable from DD12 at the outer edge of the optic vesicles, corresponding to the spatiotemporal expression in the native mouse retinal development[34]. The expression of Fstl4::Venus was faint at DD12 and enhanced from DD14 with non-uniform expression in some of the subpopulation. This finding may mimic the expression observed in the native developing retinas[33]. From DD14 to 20, we found most Brn3a-positive cells co-expressed Fstl4::Venus (Figure 1F).

In conventional retinal SFEBq culture, optic vesicles were isolated at DD10 and placed into low-cell binding dishes in N2-supplemented DMEM/F12 medium with 10% FBS (D-F10)[14]. To induce neurite outgrowth from RGCs, we placed them on the MG-coated plates (Figure 1G). After 5 days of incubation, Venus-positive neurites extended outside optic vesicles (Figure 1H). Math5 and Islet1, transcription factors responsible for RGC development, were also positive in the nuclei of neurite-extending cells (Supplemental Figure 1).

Optimization of culture condition suitable for neurite extension from the mouse Fstl4::Venus RGCs

To obtain adequate amounts of longer RGC neurites from the optic vesicles placed on MG-coated plates, we first optimized the appropriate time points for the

placement. The optic vesicles were isolated and placed every 2 or 3 days, and the total amount of the neurites was quantified for 5 days after placement (DAP) (Figure 2A). The optic vesicles placed between DD12 and 17 had more and longer neurites than those placed at DD10 and 20 (Figure 2B and C). In DD10 optic vesicles, a small number of distinct neurites was observed, while in the DD20 optic vesicle, neurite outgrowth was almost undetectable (Figure 2B and C).

Following this, we optimized the MG coating and culture medium. The isolated optic vesicles were placed on thicker (100%) and thinner (10%) MG-coated plates, containing four different culture media with different FBS concentrations and supplements that were reported to be suitable for primary RGC cultures (Figure 2D). In the case of the thicker MG coating, neurites radially spread in a linear manner in the DMEM/F12-based media. However, after extension, an atrophic phenotype with thinner neurites was observed in the media with lower FBS concentrations (Figure 2E); the incidence rates of neurite atrophy per optic vesicles were 60% in D-F10, 75% in D-F1, 89% in D-F0, and 0% in N-B27 at 5 DAP. The neurite atrophy in the D-F10 medium suggested that DMEM/F12-based media were not suitable for maintaining neurites. On the other hand, optic vesicles cultured in N-B27 showed the extension of more neurites without any atrophic phenotype. These neurites radially spread, but extended in a winding manner. In the case of the thinner MG coating, cells displaying glia-like polygonal morphology (glia-like cells) robustly migrated to the outside of the optic vesicles in FBS-containing DMEM/F12-based media (the incidence rates at 5 DAP: D-F10 60%, D-F1 88%, D-F0 33%, and N-B27 22%). In the N-B27 medium, the neurites formed bundles, and the neighboring bundles connected to one another outside the optic vesicles (Figure 2D and 3B).

To examine the time course of RGC neuritogenesis, we quantified the

number and length of the neurites on the thicker MG-coated series, where no glia-like cells were observed. In any DMEM/F12-based media (D-F10, D-F1, and D-F0), the number of the grown neurites were saturated to approximately 150 per sphere by 5 DAP (Figure 2F). Neuritogenesis in medium with higher FBS concentrations appeared to be delayed. In the N-B27 medium, we observed approximately twice the number of neurites than that in DMEM/F12-based media (Figure 2F). For neurite length, we measured the three longest neurites in each group because a number of neurites in any DMEM/F12-based media showed an atrophic phenotype (Figure 2G). Although the neurites in DMEM/F12-based media could reach a length of approximately 1 mm, longer neurites in the N-B27 medium were observed. We further reconfirmed the appropriate time point of the placement of optic vesicles into the N-B27 medium. The optimal time point for placement was DD12–17, which was comparable with that for placement for DMEM/F12-based media (Supplemental Figure 2).

To further examine Venus-positive RGC neurites cultured in the N-B27 medium, immunohistochemical analyses were performed with antibodies for beta-III tubulin, a neuron-specific cytoskeletal protein, and SMI312, a pan-axonal neurofilament marker (Figure 3A and B). Colocalization of beta-III tubulin and SMI312 in neurites was observed, indicating that all neurites outside the optic vesicles showed axonal characteristics. In the case of the thicker MG coating, the Venus protein visualized a partial fraction of the outgrown neurites, verifying that functionally distinctive subsets of RGCs were differentiated in the 3D-retinas (Figure 3A).

Optimization of culture condition suitable for neurite extension of RGCs differentiated from the human ESCs

To further expand the human RGC studies, we optimized the culture procedure suitable for RGCs differentiated from human ESCs. We first performed section immunohistochemistry with pan-RGC markers (BRN3A and BRN3B) of approximately DD46 3D-retinas differentiated by the modified human retinal SFEBq culture procedure[32] (Figure 4A–C). We confirmed that these marker expressions were comparable with those in previously reported methods[31].

Following this, we optimized the culture procedure by placing the DD46 optic vesicles on either thinner or thicker MG-coated plates in various culture media. First, we tested culture media containing FBS (D-F10, D-F1, and D-F0). As observed in the mouse RGC culture, the neurites showed atrophic phenotypes in the case of the thicker MG coating (Figure 4D upper panels and E; the incidence rates at 7 DAP: D-F10 29%, D-F1 57%, D-F0 100%, D-B27 29%, and N-B27 14%). The glia-like cells were detected on the thinner MG coating (the incidence rates at 7 DAP: D-F10 100%, D-F1 100%, D-F0 17%, D-B27 17%, and N-B27 0%), although neurites were visible in comparison with those of the mouse RGCs (Figure 4D lower left and middle panels). We then examined B27-supplemented media. In the case of the thicker MG coating, neurite outgrowth and maintenance were improved in the D-B27 and N-B27 (Figure 4F, upper panels). These neurites formed bundles; however, they radially spread linearly with less connection to the neighboring bundles. On the thinner MG coating, longer neurites extended further than those on the thicker MG coating, forming bundles that linearly spread and were connected to each other (Figure 4F, lower panels). In the D-B27 medium, up to 4 mm of bundled neurites were observed (Figure 4F and G).

Furthermore, we estimated neuritogenesis in number and length. The B27-supplemented media (D-B27 and N-B27) caused a significant increase in the number of outgrown neurites at 4.5 and 7 DAP (Figure 4H). The length of the three longest neurites in each group on both the thicker and thinner MG coating (Figure 4I and J) indicated that longer neurites could be particularly observed in B27-supplemented media. This finding strongly suggested that the B27 supplement is required for human RGC neuritogenesis and maintenance.

Using whole-mount fluorescent immunohistochemistry, the neurites from placed optic vesicles were double-labeled with beta-III tubulin and SMI312 (Figure 5). In the D-F10 medium with the thicker MG coating, immunostained signals were preferentially detected on the surface of the optic vesicles, while the neurites cultured in any B27-supplemented media grew outside the vesicles. In the D-F10 medium with the thinner MG coating, the neurites traversed the glia-like cells that had migrated outside the vesicles (Figure 5, lower left panel).

DISCUSSION

When *in vitro* differentiated RGCs are studied, it is important to (1) verify differentiation status of RGCs and (2) clearly visualize and maintain the neurite outgrowth. Organotypic cultures by isolating living animals are more advantageous than dissociated single-cell culture because the tissue environment such as differentiated cell types, retinal neurons, intercellular connectivity, and extracellular components is retained[35]. However, because these procedures require living animals at each developmental time point of interest, it was not practical to use this type of model for precise developmental analyses such as embryonic RGC studies. We would face difficulties with this type of testing in human models. Recently, several

methods to differentiate RGCs from embryoid bodies of mouse or human pluripotent stem cells have been proposed and have confirmed the expression of Brn3, a differentiation marker of RGCs[10-13]. The modified retinal SFEBq culture provided 3D-retinas with laminated retinal neurons[14,29]. In this study, we observed Fstl4-expressing RGCs in the 3D-retinas, strongly indicating that RGCs in the optic vesicles are differentiated at the subtype level. Thus, our 3D-retinas would be ideal for RGC studies.

In our 3D-retinas, co-expressions of Brn3a and Fstl4::Venus were observed. However, considering that both Brn3a and Fstl4 are expressed in the subpopulation of RGCs[15,33], a concern remains regarding the possible existence of non-RGC neurites without Venus- nor Brn3a-expression, although both Venus-positive and -negative neurites indicated similar morphology. To reduce this possibility, we isolated optic vesicles with strong Venus fluorescence. These would correspond to the dorsotemporal region of the native mouse retinas where Fstl4-positive RGCs are densely distributed[33]. Thus, in this study, almost all of the neurites were Fstl4::Venus-positive.

To visualize and maintain the neurite outgrowth from the 3D-retinas, we manipulated the timing of the excision and placement, culture media, and biological coating. The most suitable combinations in mouse and human models are listed in Table 1.

The timing of placement has been considered in organotypic culture of mouse RGCs. To grow many neurites from RGCs, it was common that retinal tissues were dissected in the last embryonic week[36-38]. This trend was reproducible in the 3D-retinas. Placement from DD12 to DD17 resulted in good neuritogenesis, which is consistent with the developmental window of the native mouse RGCs[39]. The optic

vesicles isolated at DD20 showed lesser and shorter neuritogenesis. Considering that RGCs at DD20 are localized at the outer edge of optic vesicles, they would be damaged before placement. In the human retina, RGC development begins from postconceptional day (PCD) 38 and peaks at PCD 52[40]; therefore, it would be reasonable to place the human optic vesicles at DD46.

In the medium selection after placement, we tested the maturation media used in the conventional 3D-retinal differentiation protocol[14] (D-F10 and D-F0) as well as the media preferentially used in the mouse explant culture[4,38] (N-B27 and D-B27). In the media of D-F1 as well as in D-F10 and D-F0, neuritogenesis was observed; however, atrophic phenotype or glia-like cells emerged depending on the MG coating within 5 DAP. On the other hand, N-B27 and D-B27 media preserved the outgrown neurites without the proliferation of glia-like cells; this suggests that the B27 supplement, commonly used for retinal explant culture, is suitable for RGC culture. FBS would not be sufficient to maintain the grown neurites but would promote glial proliferation similar to glial cells in primary retinal and central nervous system neuronal cultures[38,41]. In the human model, Neurobasal-A as well as DMEM/F12/N2 was acceptable.

In the biological coating, poly-D-lysine, collagen, laminin, and Matrigel have been selected to promote and preserve the neuritogenesis of RGCs from retinal explants[3,4,42-44]. In our optimization, we focused on Matrigel because biological coating with a single molecule insufficiently promoted neurite outgrowth (data not shown). Our results showed significant neurite outgrowth in both mouse and human models. Matrigel is composed of laminin, collagen type IV, entactin, and heparan sulfate proteoglycan (HSPG) and contains bFGF, NGF, and TGF beta. Laminin is known as a major component of the inner limiting membrane of the retina[45], and was

reported to promote neurite outgrowth of the retinal explants[46]. Considering that HSPG is restricted to the inner surface of the developing mouse retina[47], and that HSPG-supported bFGF signaling regulates axonal pathfinding during RGC development[48,49], HSPG in Matrigel would play a role in expanding neurites outside the optic vesicles. The optic vesicles in the 3D-retinas, which are floating on the culture medium and do not have vitreum, would have less laminin and/or HSPG on the surface of the RGC layer. This could be attributed to better neuritogenesis because of Matrigel in the 3D-retinas.

We optimized culture systems to assess the neurite outgrowth of RGCs from 3D-retina-like tissues differentiated from mouse and human ESCs without the purification process. These culture conditions require further modifications depending on the purpose. However, the present method may provide quantitative evaluation of RGC-neurite viability, outgrowth, and projections, which are suitable for pathophysiological and pharmacological studies also applicable to human RGCs.

Acknowledgments

We would like to express our appreciation to Dr. Yoshiki Sasai for providing *Rx::*Venus and *Crx::*Venus human ESCs. We received generous support from all members of the Takahashi Laboratory. Y.M. is deeply grateful for the assistance of Yuko Iwasaki (image analysis), Hiromi Ito and Kaori Ueda (technical assistance), David Atwood (image editing), and Momo Fujii and Tomoyo Hashiguchi (technical advice). This work was supported in part by grants from the Research Center Network for Realization of Regenerative Medicine (MEXT), JSPS KAKENHI (Grant Number 24687010), and Kato Memorial Bioscience Foundation.

Declaration of interest

The authors report no conflicts of interest. The authors alone are responsible for the content and writing of the paper.

References

1. Isenmann S, Kretz A, Cellerino A. Molecular determinants of retinal ganglion cell development, survival, and regeneration. Prog Retin Eye Res. 2003;22:483–543.
2. Seigel GM. The golden age of retinal cell culture. Mol Vis. 1999;5:4.
3. Smalheiser NR, Crain SM. Formation of functional retinotectal connections in co-cultures of fetal mouse explants. Brain Res. 1978;148:484–492.
4. Gaublomme D, Buyens T, Moons L. Automated analysis of neurite outgrowth in mouse retinal explants. J Biomol Screen. 2013;18:534–543.
5. Wassle H, Boycott BB. Functional architecture of the mammalian retina. Physiol Rev. 1991;71:447–480.
6. Levin LA, Gordon LK. Retinal ganglion cell disorders: types and treatments. Prog Retin Eye Res. 2002;21:465–484.
7. Hu DN, Ritch R. Tissue culture of adult human retinal ganglion cells. J Glaucoma. 1997;6:37–43.
8. Niyadurupola N, Sidaway P, Osborne A, Broadway DC, Sanderson J. The development of human organotypic retinal cultures (HORCs) to study retinal neurodegeneration. Br J Ophthalmol. 2011;95:720–726.
9. Fernandez-Bueno I, Fernandez-Sanchez L, Gayoso MJ, Garcia-Gutierrez MT, Pastor JC, Cuenca N. Time course modifications in organotypic culture of human neuroretina. Exp Eye Res. 2012;104:26–38.
10. Jagatha B, Divya MS, Sanalkumar R, Indulekha CL, Vidyanand S, Divya TS, et al. In vitro differentiation of retinal ganglion-like cells from embryonic stem cell derived neural progenitors. Biochem Biophys Res

Commun. 2009;380:230–235.

11. Parameswaran S, Balasubramanian S, Babai N, Qiu F, Eudy JD, Thoreson WB, et al. Induced pluripotent stem cells generate both retinal ganglion cells and photoreceptors: therapeutic implications in degenerative changes in glaucoma and age-related macular degeneration. Stem Cells 2010;28:695–703.
12. Riazifar H, Jia Y, Chen J, Lynch G, Huang T. Chemically induced specification of retinal ganglion cells from human embryonic and induced pluripotent stem cells. Stem Cells Transl Med. 2014;3:424–432.
13. Xie BB, Zhang XM, Hashimoto T, Tien AH, Chen A, Ge J, et al. Differentiation of retinal ganglion cells and photoreceptor precursors from mouse induced pluripotent stem cells carrying an Atoh7/Math5 lineage reporter. PLoS One 2014;9:e112175.
14. Eiraku M, Takata N, Ishibashi H, Kawada M, Sakakura E, Okuda S, et al. Self-organizing optic-cup morphogenesis in three-dimensional culture. Nature 2011;472:51–56.
15. Xiang M, Zhou L, Macke JP, Yoshioka T, Hendry SH, Eddy RL, et al. The Brn-3 family of POU-domain factors: primary structure, binding specificity, and expression in subsets of retinal ganglion cells and somatosensory neurons. J Neurosci. 1995;15:4762–4785.
16. Mu X, Klein WH. A gene regulatory hierarchy for retinal ganglion cell specification and differentiation. Semin Cell Dev Biol. 2004;15:115–123.
17. Badea TC, Cahill H, Ecker J, Hattar S, Nathans J. Distinct roles of transcription factors brn3a and brn3b in controlling the development, morphology, and function of retinal ganglion cells. Neuron 2009;61:852–

864.

18. Barlow HB, Hill RM, Levick WR. Retinal Ganglion Cells Responding Selectively to Direction and Speed of Image Motion in the Rabbit. J Physiol. 1964;173:377–407.
19. Cleland BG, Levick WR. Properties of rarely encountered types of ganglion cells in the cat's retina and an overall classification. J Physiol. 1974;240:457–492.
20. Rodieck RW, Watanabe M. Survey of the morphology of macaque retinal ganglion cells that project to the pretectum, superior colliculus, and parvicellular laminae of the lateral geniculate nucleus. J Comp Neurol. 1993;338:289–303.
21. Kim IJ, Zhang Y, Meister M, Sanes JR. Laminar restriction of retinal ganglion cell dendrites and axons: subtype-specific developmental patterns revealed with transgenic markers. J Neurosci. 2010;30:1452–1462.
22. Badea TC, Nathans J. Morphologies of mouse retinal ganglion cells expressing transcription factors Brn3a, Brn3b, and Brn3c: analysis of wild type and mutant cells using genetically-directed sparse labeling. Vision Res. 2011;51:269–279.
23. Tsuchimoto M, Yasuo S, Funada M, Aoki M, Sasagawa H, Yoshimura T, et al. Conservation of novel Mahya genes shows the existence of neural functions common between Hymenoptera and Deuterostome. Dev Genes Evol. 2005;215:564–574.
24. Ying QL, Wray J, Nichols J, Batlle-Morera L, Doble B, Woodgett J, et al. The ground state of embryonic stem cell self-renewal. Nature

2008;453:519–523.

25. Kiyonari H, Kaneko M, Abe S, Aizawa S. Three inhibitors of FGF receptor, ERK, and GSK3 establishes germline-competent embryonic stem cells of C57BL/6N mouse strain with high efficiency and stability. Genesis 2010;48:317–327.
26. Osakada F, Ikeda H, Mandai M, Wataya T, Watanabe K, Yoshimura N, et al. Toward the generation of rod and cone photoreceptors from mouse, monkey and human embryonic stem cells. Nat Biotechnol. 2008;26:215–224.
27. Wataya T, Ando S, Muguruma K, Ikeda H, Watanabe K, Eiraku M, et al. Minimization of exogenous signals in ES cell culture induces rostral hypothalamic differentiation. Proc Natl Acad Sci U S A. 2008;105:11796–11801.
28. Homma K, Okamoto S, Mandai M, Gotoh N, Rajasimha HK, Chang YS, et al. Developing rods transplanted into the degenerating retina of Crx-knockout mice exhibit neural activity similar to native photoreceptors. Stem Cells 2013;31:1149–1159.
29. Assawachananont J, Mandai M, Okamoto S, Yamada C, Eiraku M, Yonemura S, et al. Transplantation of embryonic and induced pluripotent stem cell-derived 3D retinal sheets into retinal degenerative mice. Stem Cell Reports 2014;2:662–674.
30. Gonzalez-Cordero A, West EL, Pearson RA, Duran Y, Carvalho LS, Chu CJ, et al. Photoreceptor precursors derived from three-dimensional embryonic stem cell cultures integrate and mature within adult degenerate retina. Nat Biotechnol. 2013;31:741–747.

31. Nakano T, Ando S, Takata N, Kawada M, Muguruma K, Sekiguchi K, et al. Self-formation of optic cups and storable stratified neural retina from human ESCs. Cell Stem Cell 2012;10:771–785.
32. Kuwahara A, Ozone C, Nakano T, Saito K, Eiraku M, Sasai Y. Generation of a ciliary margin-like stem cell niche from self-organizing human retinal tissue. Nat Commun. 2015;6:6286.
33. Yonehara K, Shintani T, Suzuki R, Sakuta H, Takeuchi Y, Nakamura-Yonehara K, et al. Expression of SPIG1 reveals development of a retinal ganglion cell subtype projecting to the medial terminal nucleus in the mouse. PLoS One 2008;3:e1533.
34. Quina LA, Pak W, Lanier J, Banwait P, Gratwick K, Liu Y, et al. Brn3a-expressing retinal ganglion cells project specifically to thalamocortical and collicular visual pathways. J Neurosci. 2005;25:11595–11604.
35. Caffe AR, Ahuja P, Holmqvist B, Azadi S, Forsell J, Holmqvist I, et al. Mouse retina explants after long-term culture in serum free medium. J Chem Neuroanat. 2001;22:263–273.
36. Horie H, Ito S, Takano M. Regional differences in neurite regeneration of postnatal mouse retinal explants. Brain Res Bull. 1994;34:381–384.
37. Tsai RK, Sheu MM, Wang HZ. Capability of neurite regeneration of rat retinal explant at different ages. Kaohsiung J Med Sci. 1998;14:192–196.
38. Wang SW, Mu X, Bowers WJ, Klein WH. Retinal ganglion cell differentiation in cultured mouse retinal explants. Methods 2002;28:448–456.
39. Marquardt T, Gruss P. Generating neuronal diversity in the retina: one for nearly all. Trends Neurosci. 2002;25:32–38.

40. Finlay BL. The developing and evolving retina: using time to organize form. Brain Res. 2008;1192:5–16.
41. Robertson PL, Goldstein GW. Heparin inhibits the growth of astrocytes in vitro. Brain Res 1988;447:341-345.
42. Smalheiser NR, Crain SM, Reid LM. Laminin as a substrate for retinal axons in vitro. Brain Res. 1984;314:136–140.
43. Bates CA, Meyer RL. The neurite-promoting effect of laminin is mediated by different mechanisms in embryonic and adult regenerating mouse optic axons in vitro. Dev Biol. 1997;181:91–101.
44. Henke-Fahle S, Wild K, Sierra A, Monnier PP. Characterization of a new brain-derived proteoglycan inhibiting retinal ganglion cell axon outgrowth. Mol Cell Neurosci. 2001;18:541–556.
45. Libby RT, Champliaud MF, Claudepierre T, Xu Y, Gibbons EP, Koch M, et al. Laminin expression in adult and developing retinae: evidence of two novel CNS laminins. J Neurosci. 2000;20:6517-6528.
46. Smalheiser NR, Crain SM, Reid LM. Laminin as a substrate for retinal axons in vitro. Brain Res 1984;314:136-140.
47. Chung KY, Leung KM, Lin L, Chan SO. Heparan sulfate proteoglycan expression in the optic chiasm of mouse embryos. J Comp Neurol. 2001;436:236–247.
48. Kim MJ, Cotman SL, Halfter W, Cole GJ. The heparan sulfate proteoglycan agrin modulates neurite outgrowth mediated by FGF-2. J Neurobiol. 2003;55:261–277.
49. Ogata-Iwao M, Inatani M, Iwao K, Takihara Y, Nakaishi-Fukuchi Y, Irie F, et al. Heparan sulfate regulates intraretinal axon pathfinding by retinal

ganglion cells. Invest Ophthalmol Vis Sci. 2011;52:6671–6679.

FIGURE LEGENDS

Figure 1. Three-dimensional retina differentiation and neurite outgrowth of optic vesicles differentiated from Fstl4::Venus mouse ESCs

(A) Phase-contrast micrograph of feeder-free culture of Fstl4::Venus-knock-in mouse ESCs. Scale bar: 100 μm.

(B) RT-PCR detected the expression of Nanog, Oct4, Rx, and G3pdh (endogenous control) before differentiation and at differentiation day (DD) 10 and DD23 from Fstl4::Venus mouse ESCs.

(C) Section immunohistochemistry of the DD20 optic vesicle differentiated from Fstl4::Venus mouse ESCs, stained with the Rhodopsin (red) antibody and DAPI (blue). Scale bar: 50 μm.

(D–E) Developmental images of the 3D-retinas from the Fstl4::Venus ESCs. Optical (D) and fluorescence (E) micrographs of the 3D-retinas from DD10 to DD20 were shown. Scale bar: 200 μm.

(F) Venus (green) and Brn3a (red) fluorescence during 3D-retina differentiation, as shown in confocal microscopic images of immunohistochemistry in optic vesicles between DD10 and DD20, counter-stained with DAPI (blue) for nuclei. Magnified views of the area surrounded by white squares were located under the left-lower of former images at DD12 to DD20. Scale bar: 50 μm in main images and 10μm in magnified images.

(G) The schematic diagram of the procedure for 3D-retina differentiation from mouse ESCs and neurite outgrowth. SFEBq; serum-free floating culture of embryoid body-like aggregates with quick reaggregation, KSR; knockout serum replacement, AGN; retinoic acid receptor antagonist AGN193109, GFR; growth factor reduced, RA; retinoic acid.

(H) Phase-contrast and fluorescent images of Venus-positive neurites from optic vesicles of differentiated 3D-retina obtained by IncuCyte (upper) and Olympus IX71 (lower). The white square represents the area of the lower panels. Scale bar: 500 μm.

Figure 2. Optimization of culture conditions for neurite extension from the mouse Fstl4::Venus RGCs

(A) Line chart of the mean number of the neurites extended in N2-supplemented DMEM/F12 medium with FBS10% (D-F10) on 100% (thicker) Matrigel (MG)-coated plates, depending on the initial differentiation day (DD).

(B) Bar graph indicating the mean number of the neurites extended at 3 days after placement (DAP) (left group) and 5 DAP (right group) in D-F10 medium on 100% (thicker) MG-coated plates.

(C) Bar graph of the mean length of three longest neurites at 5 DAP. Longer neurites extended at 5 DAP from DD12 to DD17. *$p < 0.05$.

(A–C) Values were presented as means ± standard deviation (S.D.). (DD10 n = 6, DD12 n = 5, DD14 n = 10, DD17 n = 6, DD20 n = 5).

(D) Phase-contrast micrographs of the neurites at 5 DAP in N2-supplemented DMEM/F12 medium with 10% (D-F10), 1% (D-F1), and 0% (D-F0) FBS or B27 supplemented Naurobasal-A medium (N-B27) placed on 100% (upper panels) or 10% (lower panels) MG-coated plates. Scale bar: 200 μm.

(E) Phase-contrast micrograph showing neuritric atrophy of the 2-DAP optic vesicle in D-F0 medium. Scale bar: 200 μm.

(F) The bar graph of the mean number of the neurites extended at 1, 3, and 5 DAP in various media on 100% (thicker) MG-coated plates.

(G) The bar graph of the mean length of three longest neurites per sphere at 5 DAP in various media on 100% (thicker) MG-coated plates.

(F–G) Values were presented as means ± S.D. (*p < 0.05, **p < 0.01. D-F10 n = 10, D-F1 n = 8, D-F0 n = 9, N-B27 n = 9).

Figure 3. Whole-mount immunohistochemistry of the neurites from the Fstl4::Venus optic vesicles

(A–B) The Maximum intensity projection images of whole-mount immunohistochemistry of neurites extended on thicker (A) or thinner (B) MG-coated inserts cultured in the N-B27 medium. The neurites were visualized by Venus (green), beta-III tubulin (red), and SMI312 (cyan). Lower panels indicate the higher magnification images of the areas framed by white squares in the upper panel. Scale bar: 500 µm (upper), 200 µm (lower).

Figure 4. Optimization of culture conditions suitable for neurite extension from the human *Crx*::Venus RGCs

(A) Phase-contrast (upper) and fluorescence (lower) micrographs of 3D-retina-like spheres derived from *Rx*::Venus (left) and *Crx*::Venus (right) human ESCs. Scale bar: 200µm.

(B) Confocal microscopic image of section immunohistochemistry of DD45 optic vesicles differentiated from *Rx*::venus human ESCs, costained with DAPI (blue), Brn3b (left panel, red), or Brn3a (right panel, red) as RGC markers. Scale bar: 50 µm.

(C) The schematic diagram of the procedure for 3D-retina differentiation from the human ESCs and the neurites outgrowth. gfCDM; growth factor-free chemically defined medium, BMP4; bone morphogenetic protein 4, GSK3i; glycogen synthase

kinase 3 inhibitor.

(D–F) Phase-contrast micrographs of the grown neurites. Scale bar: 200 μm.

(D) Neurites extended at 7 DAP cultured in D-F10, D-F1, and D-F0 media placed on 100% (upper) or 10% (lower) MG-coated plates.

(E) Phase-contrast micrograph showing neuritric atrophy (white arrowhead) of the neurites at 1.5 (upper) and 3 (lower) DAP in the D-F0 medium with 100% MG coating.

(F) Neurites extended at 7 DAP cultured in D-B27 and N-B27 media.

(G) Diagram tracing neurites observed at 7 DAP in the D-B27 medium with 10% MG coating. A number of neurites longer than 4 mm were observed. Scale bar: 2 mm.

(H) The bar graph of the mean number of the neurites extended at 1.5 (left), 4.5 (middle), and 7 (right) DAP in the different media.

(I) The bar graph of the mean length of three longest neurites per sphere at 7 DAP with 100% MG coating.

(J) The bar graph of the mean length of three longest neurites per sphere at 7 DAP with 10% MG coating.

(H–J) Values were presented as means ± S.D. (*$p < 0.05$, **$p < 0.01$. 100% MG n = 7, 10% MG n = 6 for each group)

Figure 5. Whole-mount immunohistochemistry of the neurites from the *Crx*::Venus optic vesicles

The maximum intensity projection images of whole-mount immunohistochemistry of neurites extended on thicker (upper) or thinner (lower) MG-coated inserts cultured in the D-F10 (left), D-B27 (middle), and N-B27 (right) media. The images of the neurites and optic vesicles visualized by beta-III tubulin (red), SMI312 (green), and

Crx::Venus (white) were merged with the images stained with DAPI (blue). Scale bar: 200 μm.

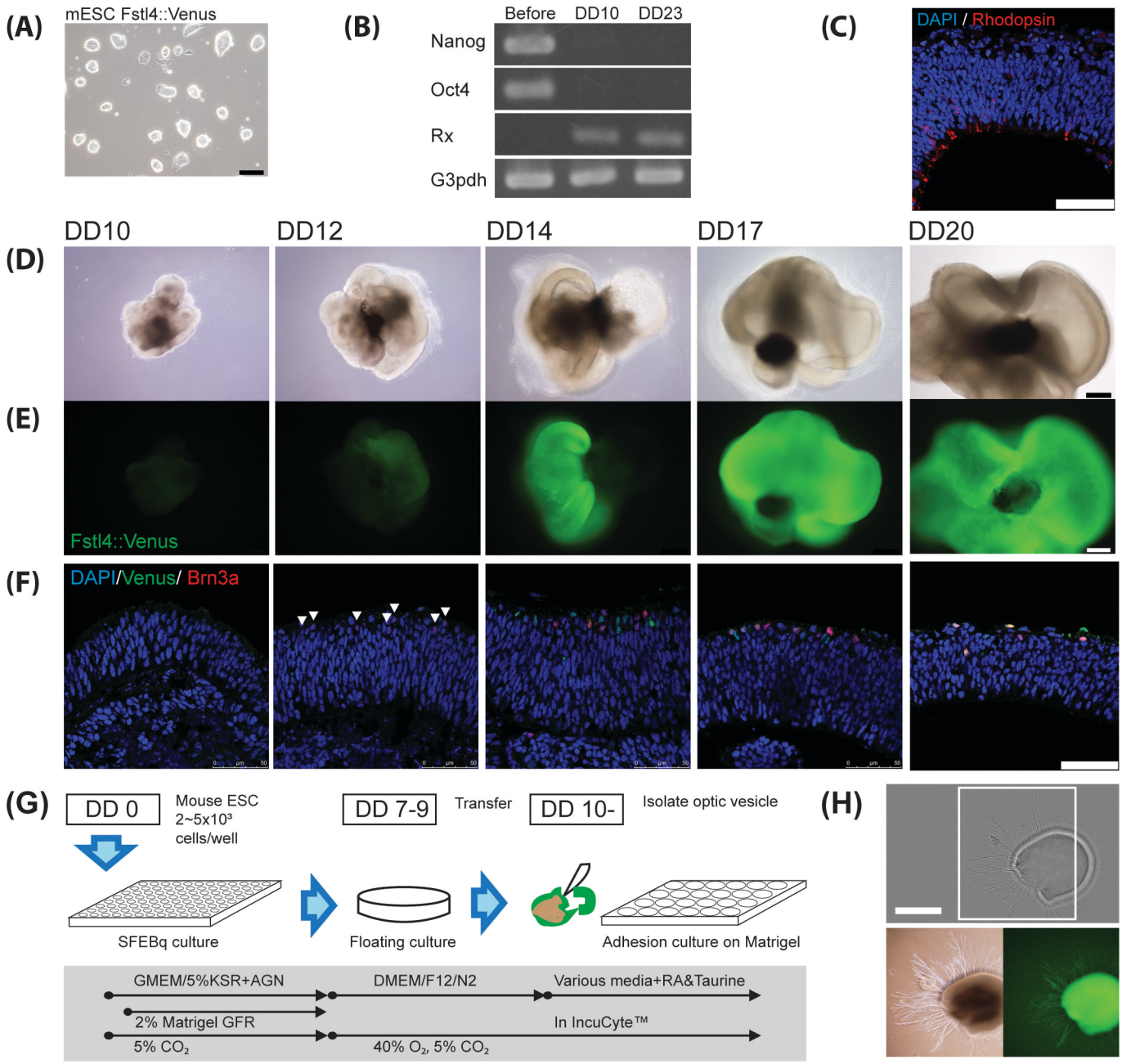

Figure 1. Maekawa et al.

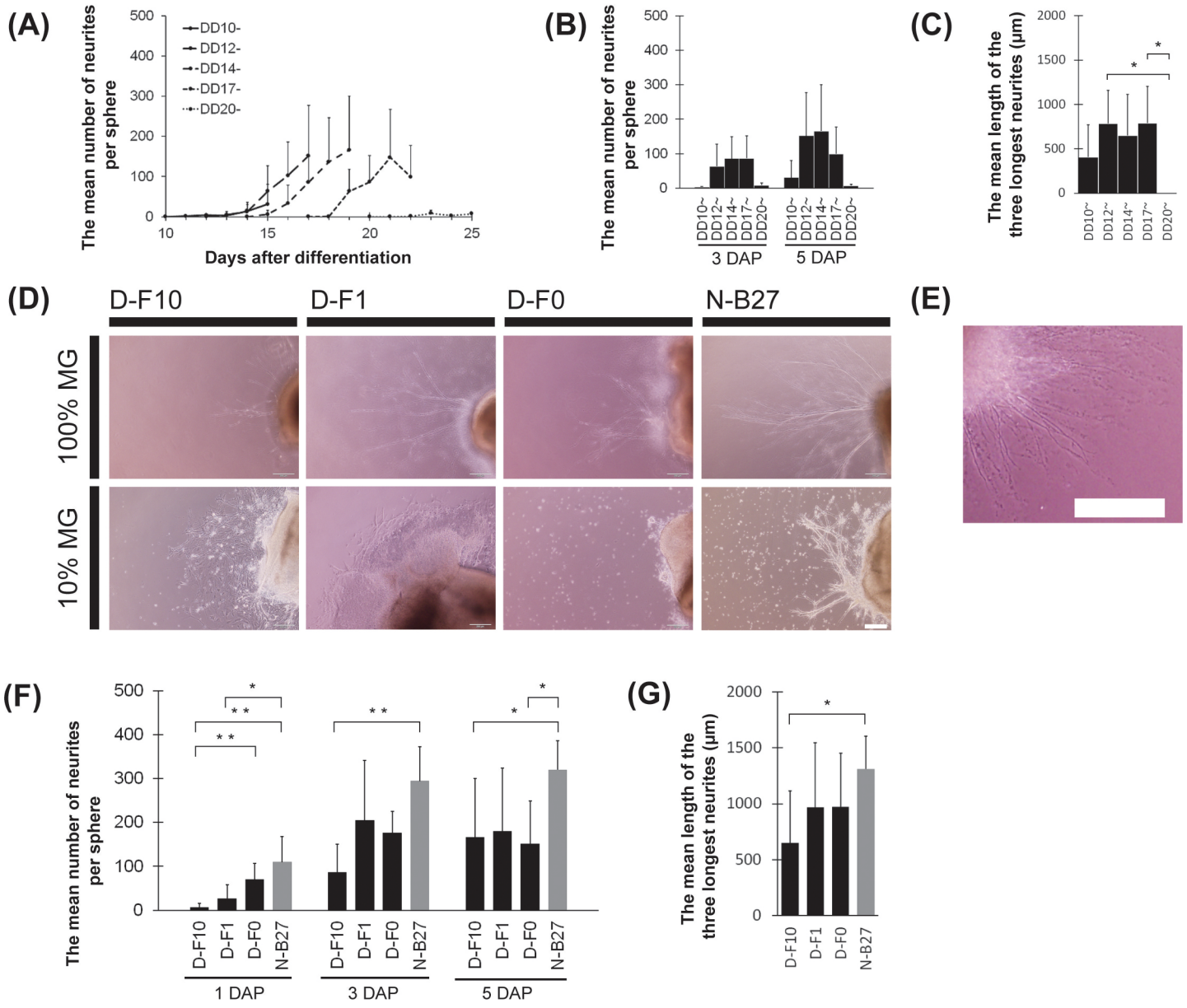

Figure 2. Maekawa et al.

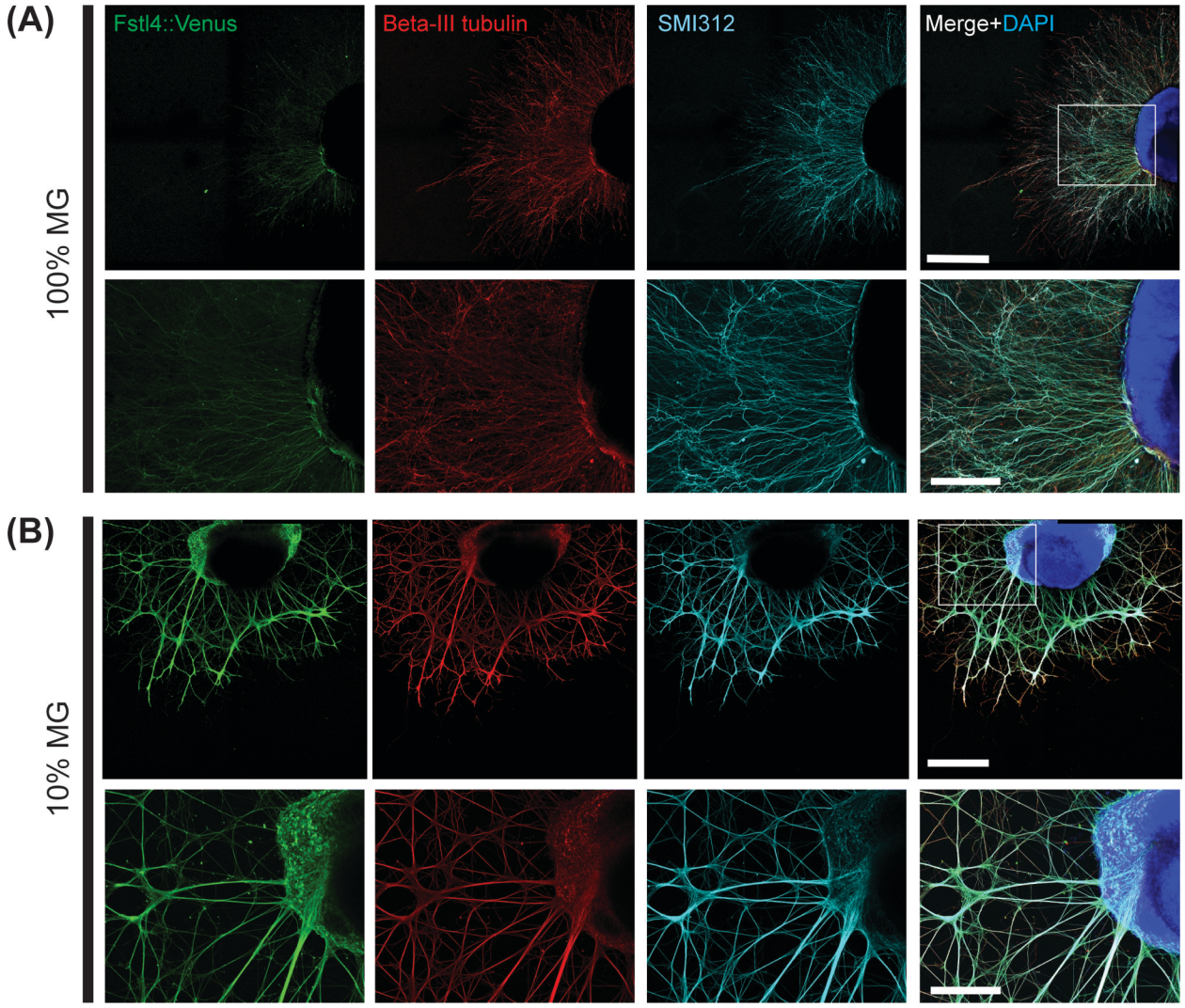

Figure 3. Maekawa et al.

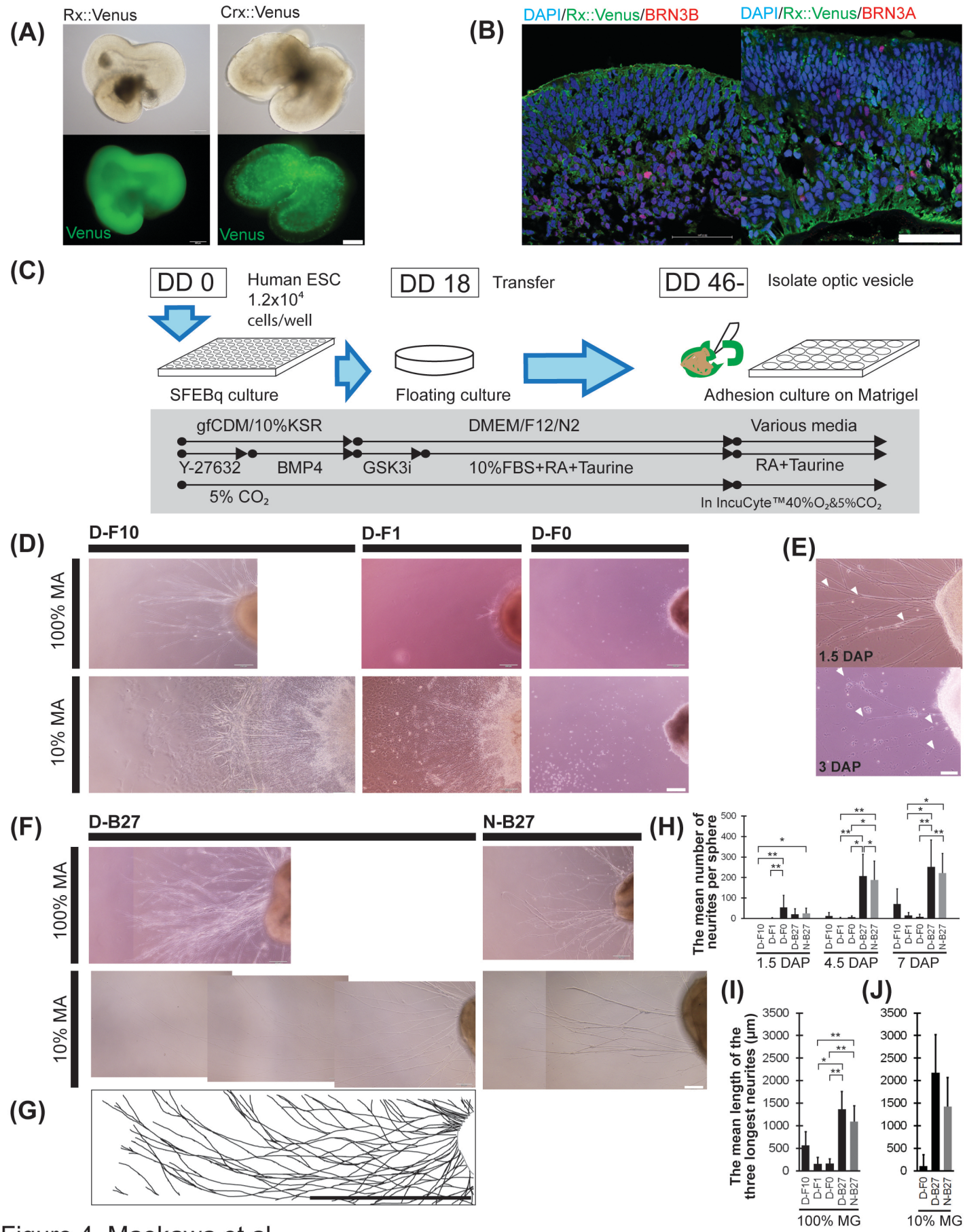

Figure 4. Maekawa et al.

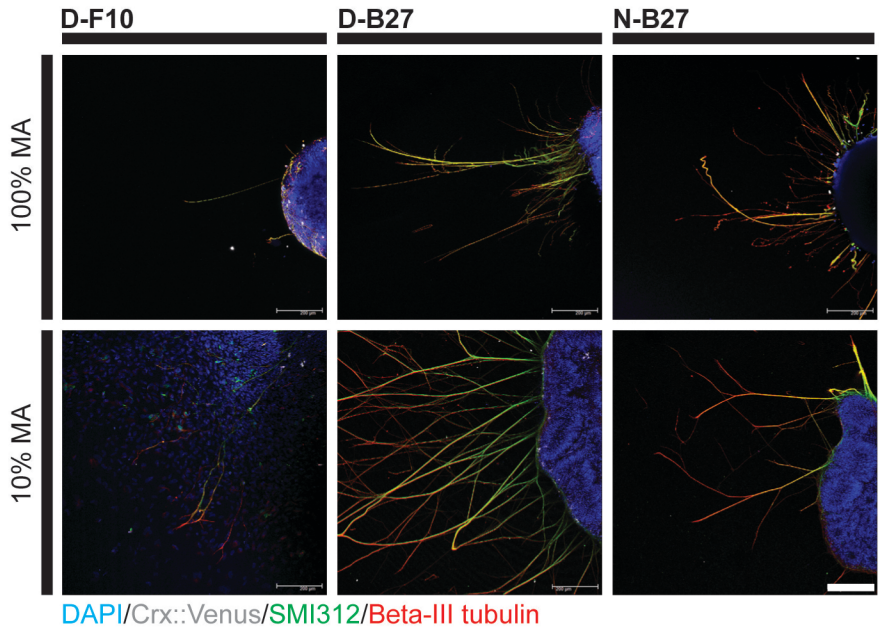

Figure 5. Maekawa et al.

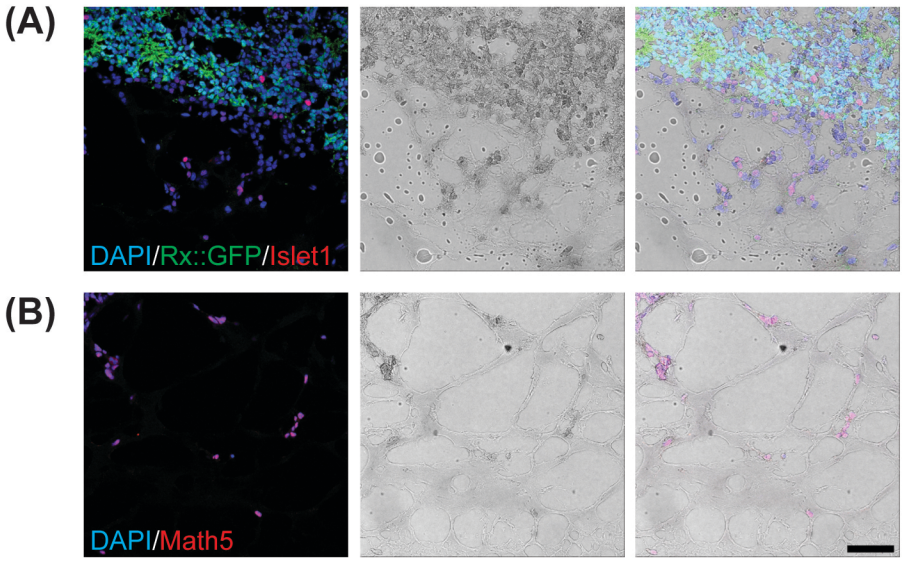

Supplemental figure 1. Maekawa et al.

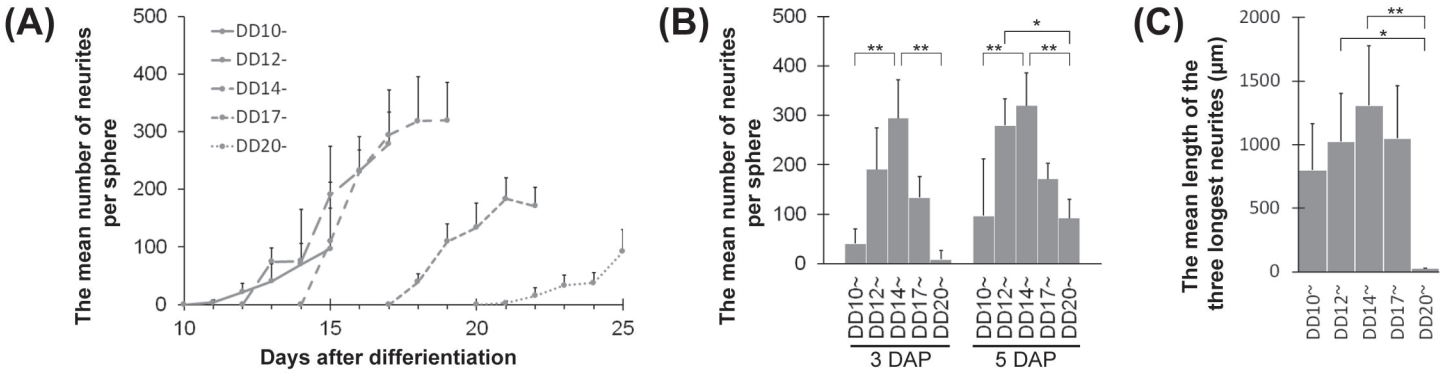

Supplemental figure 2. Maekawa et al.